

1     **Vegetation response to climate zone dynamics and its impacts on surface**  
2                                   **soil water content and albedo in China**

3     **Yanlong Guan<sup>1,2,4</sup>, Hongwei Lu<sup>1,2\*</sup>, Chuang Yin<sup>2</sup>, Yuxuan Xue<sup>1</sup>, Yelin Jiang<sup>6</sup>, Yu**  
4     **Kang<sup>2,1</sup>, Li He<sup>3,2</sup>, Janne Heiskanen<sup>4,5</sup>**

5     <sup>1</sup> Key Laboratory of Water Cycle and Related Land Surface Process, Institute of  
6     Geographic Science and Natural Resources Research, Chinese Academy of Science,  
7     Beijing, China

8     <sup>2</sup> School of Renewable Energy, North China Electric Power University, Beijing,  
9     China

10    <sup>3</sup> State Key Laboratory of Hydraulic Engineering Simulation and Safety at Tianjin  
11    University, Tianjin, China

12    <sup>4</sup> Department of Geosciences and Geography, University of Helsinki, Finland

13    <sup>5</sup> Institute for Atmospheric and Earth System Research, Faculty of Science, University  
14    of Helsinki, Finland

15    <sup>6</sup> Department of Civil and Environmental Engineering, University of Connecticut,  
16    Storrs, CT, USA

17    Corresponding author: Hongwei Lu ([luhw@igsnr.ac.cn](mailto:luhw@igsnr.ac.cn))

18

19 **Abstract**

20 Extensive research has focused on the response of vegetation to climate change,  
21 including potential mechanisms and resulting impacts. Although many studies have  
22 explored the relationship between vegetation and climate change in China, research  
23 on spatiotemporal distribution changes of climate regimes using natural vegetation as  
24 an indicator is still lacking. Further, limited information is available on the response  
25 of vegetation to shifts in China's regional climatic zones. In this study, we applied  
26 Mann–Kendall, and correlation analysis to examine the variabilities in temperature,  
27 precipitation, surface soil water, normalised difference vegetation index (NDVI), and  
28 albedo in China from 1982 to 2012. Our results indicate significant shifts in the  
29 distribution of Köppen–Geiger climate classes in China from 12.08% to 18.98%  
30 between 1983 and 2012 at a significance level of 0.05 (MK). The percentage areas in  
31 the arid and continental zones expanded at a rate of 0.004%/y and 0.12%/y,  
32 respectively, while the percentage area in the temperate and alpine zones decreased by  
33 -0.05%/y and -0.07%/y. Sensitivity fitting results between simulated and observed  
34 changes identified temperature to be a dominant control on the dynamics of temperate  
35 ( $r^2=0.98$ ) and alpine ( $r^2=0.968$ ) zones, while precipitation was the dominant control  
36 on the changes of arid ( $r^2=0.856$ ) and continental ( $r^2=0.815$ ) zones. The response of  
37 the NDVI to albedo infers a more pronounced radiative response in temperate ( $r = -$   
38  $0.82, p < 0.01$ ) and alpine ( $r = -0.476, p < 0.05$ ) compared to arid and continental  
39 zones. Furthermore, we identified more pronounced monthly increasing trends in

40 NDVI and soil water, corresponding to weak changes in albedo during vegetation  
41 growing periods. Our results suggest that climate zone shifting has considerable  
42 impacts on the vegetation in China and will have larger ecological impacts through  
43 radiative or non-radiative feedback mechanisms in future warming scenarios.

44 **Key words:** Climate zones; Temperature; Precipitation; NDVI; Albedo

## 45 **1 Introduction**

46 Research work (Carey et al., 2017; Fan and van den Dool, 2008; Shen et al., 2015;  
47 Turco et al., 2017) has demonstrated that shifts in the climate system increase the  
48 likelihood of widespread and irreversible impacts on global ecosystems, including  
49 changes to vegetation greening/coverage (Abera et al., 2019; Erb et al., 2017; Fang et  
50 al., 2004; Harris et al., 2016; Helmens et al., 2018; Huang et al., 2016; Li et al., 2018;  
51 Piao et al., 2015; Richardson et al., 2013; Shen et al., 2015; Yang et al., 2018; Zhao,  
52 2018). Vegetation supplies the materials and energy required to sustain life on Earth  
53 through photosynthesis by converting water and carbon dioxide to oxygen and  
54 carbohydrates. The length of the growing season and vegetation productivity are  
55 highly sensitive to changes in climate (Erasmí et al., 2017; Martín-Benito and  
56 Pederson, 2015; Turco et al., 2017). Greening and browning are measured by the  
57 NDVI changes, which are commonly correlated to vegetation productivity and  
58 biomass. These vegetation changes can alter the regional energy, carbon, and water  
59 balance, resulting in atmospheric warming or cooling, depending on the relative

60 impacts of radiative (albedo) and non-radiative processes (such as evapotranspiration  
61 and surface roughness length) (Abera et al., 2019; Li et al., 2015).

62 Many studies have explored the response mechanisms between climate change and  
63 vegetation processes at different scales. For example, in the context of global  
64 warming, increased vegetation productivity in the Arctic was shown to reduce surface  
65 albedo, resulting in positive temperature feedback (Pearson et al., 2013; Pithan and  
66 Mauritsen, 2014). Conversely, analysis of NDVI and evapotranspiration in the  
67 Tibetan Plateau inferred reduced surface warming in the growing season in response  
68 to increased vegetation activity (Shen et al., 2015). Gottfried et al. (2012) and Pauli et  
69 al. (2012) identified a link between ongoing continent-scale climate change and  
70 changing mountain plant communities, with a particular increase in the number of  
71 warm-adapted species due to thermophilization. Wu et al. (2015) applied NDVI and  
72 climatic data to demonstrate that the time-lag effect between vegetation and primary  
73 climate factors influences vegetation growth on a global scale.

74 The Köppen–Geiger classification (Peel et al., 2007; Rubel & Kottek, 2010) is often  
75 used to describe highly heterogeneous climate zones with different climatic  
76 conditions. It is one of the most widely accepted climate classification systems used to  
77 describe vegetation distribution based solely on annual and monthly temperature and  
78 precipitation patterns. The Köppen–Geiger criteria has been validated by a number of  
79 studies through its strong links between climate and biome type (Engelbrecht and  
80 Engelbrecht, 2016; Farmer and Cook, 2013; Rohli et al., 2015a), suggesting that its

81 dynamic characteristics still have significant research value in many fields of research  
82 today. This connection between climate and biomes provides the possibility of  
83 assessing the relationship between the empirical climate and natural vegetation (Guan  
84 et al., 2020; Guetter and Kutzbach, 1990).

85 Considering the nature of the climate classification, the change in vegetation response  
86 to climate should be presented simply and clearly. Garcia et al. (2014) reported that  
87 changes in the regional distribution of climate can affect the availability and  
88 distribution of climatically suitable areas for vegetation. The changes in specific  
89 climate zones suitable for the vegetation types are likely to result in the expansion or  
90 reduction of the distribution range of specific vegetation types. Rohli et al. (2015a)  
91 identified that the boundaries of the Köppen classes strongly overlapped with many  
92 ecological factors, such as vegetation distribution. Williams et al. (2007) suggested  
93 that novel and disappearing climates can lead to the disaggregation of vegetation  
94 species assemblages. Wang and Overland, (2004) reported a decline in the Arctic  
95 Tundra climate zone since the 1990s, accompanied by a marked increase in boreal and  
96 temperate groups. According to modelling results by Pearson et al. (2013), at least  
97 half of the Arctic vegetation coverage is expected to shift by 2050, with woody  
98 vegetation coverage expected to increase by 52% in response to specific climate  
99 change. In some areas where the tundra is replaced by shrubs, the albedo in the  
100 growing season will decrease.

101 Recent studies have shown that we can hypothesise that if shifts between climate  
102 zones occur constantly, vegetation will substantially respond to shifting climate zones  
103 and surface biophysical characteristics will change. Similar to changes in land cover,  
104 shifts in heterogeneous climate zones are highly likely to affect vegetation structure  
105 (e.g., canopy height), phenology, the seasonality of albedo, and even vegetation type  
106 succession, which in turn directly affect regional surface energy balance and net  
107 radiation partitioning (Richardson et al., 2013). However, the impacts of shifting  
108 climate zones on vegetation have not yet been fully addressed in China. In this regard,  
109 the combination of NDVI, soil water, and albedo variables can be effectively used to  
110 shed light on the impact of shifting climate zones on vegetation, further its surface  
111 biophysical characteristics. Thus, further examination using relatively high-resolution  
112 remote sensing observations and reanalysis data sets is needed, in the area that have  
113 undergone climate type shifts, to better understand the impact of temperature and  
114 precipitation to specific climate zones, and to clarify the potential response of  
115 vegetation to specific climate zones.

116 This study aims to determine the dynamic response of regional vegetation in China to  
117 the shifting climatic regimes and its resulting impact on surface biophysical  
118 characteristics from 1982 to 2012. In particular, we explored (1) the temporal shifts of  
119 the Köppen climate regions, including total climate zones, and specific arid,  
120 temperate, continental, and alpine climate regions; (2) the dominant drivers  
121 (temperature or precipitation) of the dynamics of specific climate zones; and (3) the

122 response of vegetation to changes in the four climate zones and its influence on  
123 surface soil water (SW) content and albedo. The exploration between vegetation  
124 response and the climate types involved can better estimate the uniqueness of climate  
125 change at a given scale, and may also inform our understanding of impacts of climate  
126 change on biome.

## 127 **2 Study area**

128 China's climate is complex and diverse and is predominantly controlled by the  
129 distribution of temperature (Figure 1a), precipitation (Figure 1b), and topography  
130 (Figure 1c). The spatial distribution of temperature is primarily influenced by latitude  
131 and altitude (e.g., from Qinghai to the Tibetan Plateau) and ranges from  $-12.4$  to  
132  $25.07$  °C. The total precipitation gradually decreases from a maximum of 1937.5 mm  
133 in the southeast to a minimum of 8.3 mm in the northwest. During the warm season,  
134 the southern and eastern regions of China experience high rainfall due to the influence  
135 of the monsoon. In contrast, Northwest China experiences low precipitation due to its  
136 distance from the ocean. During the cold seasons, continental circulation causes most  
137 regions, particularly in the north and west, to be cold and dry. In general, China's  
138 climate is geographically distinct and seasonally variable.

139 Given that climate is an important limiting factor in ecological processes, China's  
140 large spatial climate variability promotes the heterogeneous distribution of vegetation  
141 types and ecosystems (Figure 1d). China has a variety of land vegetation types,

142 including shrubs, swamps, broadleaf forests, meadows, coniferous forests, cultivated  
143 vegetation, alpine vegetation, grasslands, mixed forests, and deserts. From individual  
144 forms to spatial community distributions, vegetation is dependent on the temporal and  
145 spatial distribution of regional hydrothermal conditions.

146

-----

147

**Place Figure 1**

148

-----

### 149 **3 Data and methods**

#### 150 3.1 Observed and reanalysis data

151 We utilised satellite-based vegetation data, climatic observational grid data, and  
152 reanalysis data from 1982 to 2012, including NDVI, temperature, precipitation,  
153 albedo, and surface volumetric SW (Table 1). To achieve a consistent spatial  
154 resolution for the analysis, we applied the bilinear method to interpolate the remote  
155 sensing and reanalysis data to regular  $0.125^\circ \times 0.125^\circ$  grids. To further reduce the  
156 impact of natural variability, a 5-year running mean was applied to all datasets to  
157 mitigate possible short-term variations (Mahlstein et al., 2013).

158 NDVI is an effective measurement of the photosynthetically active radiation absorbed  
159 by chlorophyll in the green leaves of vegetation canopies (Pinzon & Tucker, 2014).



160 Absorption in the visible spectral region and reflectance in the near infra-red region  
161 increases with increasing chlorophyll content, leaf area index (LAI), and healthy leaf  
162 structure, and thus greener and denser vegetation will result in relatively high NDVI  
163 (approaching one). We used the GIMSS NDVI3g (v0) dataset generated from the  
164 National Oceanic and Atmospheric Administration Advanced Very High Resolution  
165 Radiometer (AVHRR) (Tucker et al., 2005; Pinzon & Tucker, 2014). The data range  
166 from July 1982 to December 2011, has a resolution of 0.0833° and is carefully  
167 harmonised from different AVHRR sensors. Negative influences, such as calibration  
168 loss, volcanic eruptions, and orbital drift, were considered in data processing.

169 Albedo and volumetric soil water (SW) reanalysis data were obtained from the  
170 European Centre for Medium-Range Weather Forecasts. The reanalysis data were  
171 produced by combining weather forecast models with observations using data  
172 assimilation, that is, the four-dimensional variational assimilation (4D-Var) method  
173 (Dee et al., 2011). In general, this is an incremental and iterative method to minimise  
174 a cost function to reduce the biases between observed values and the available short-  
175 range forecasts (Flemming et al., 2015). These datasets have been produced and  
176 archived on a reduced Gaussian grid, which has quasi-uniform spacing across the  
177 globe. Specifically, reduced Gaussian grids have a series of evenly spaced data grids  
178 along each latitude, which are spaced at quasi-regular intervals. Close to the equator,  
179 there are many points along a latitude parallel, but near the pole, only a few points  
180 along a latitude parallel. Furthermore, the datasets were interpolated to a regular grid

181 at a horizontal resolution of  $0.125^\circ$ . The default interpolation method is bilinear for  
182 our continuous parameters (e.g., albedo and SW). For SW data, we used the surface  
183 layer at a range of 0–7 cm, as surface soil moisture affected by temperature and  
184 precipitation is sensitive to vegetation change (McColl et al., 2017). For albedo data,  
185 in the short-wave radiation scheme, the surface reflection is handled by combining  
186 direct and diffuse radiation. Over land, surface albedo is derived from the monthly  
187 mean climatology of its visible and near-infrared direct and diffuse components built  
188 from MODIS albedo over the years 2000-2003 (Park, 2010; Schaaf et al., 2002). It  
189 can be used to assess potential environmental impacts from vegetation changes in  
190 different climatic regions, such as impacts on the regional energy balance.

191 China's ground temperature and precipitation grid datasets (V2.0) at  $0.5^\circ \times 0.5^\circ$   
192 resolution were provided by the National Meteorological Information Center of the  
193 China Meteorological Administration. The data cover most of China, excluding  
194 Taiwan, with 2472 national-level meteorological observation stations. Topography  
195 and vegetation type datasets were provided by the Geospatial Data Cloud  
196 (<http://www.gscloud.cn/>) and Resource and Environmental Data Clouds Platform  
197 from the Chinese Academy of Science (<http://www.resdc.cn>), respectively. These  
198 datasets have been widely applied in regional climate change research in China (Ren  
199 et al., 2015), and they provided accurate data for mapping the spatial distribution of  
200 Köppen–Geiger climatic types in the present study. We also collected monthly  
201 gridded precipitation and temperature datasets at  $0.5^\circ \times 0.5^\circ$  resolution from the

202 University of East Anglia Climatic Research Unit (CRU TS V.4.02) (Harris et al.,  
203 2014) to generate the Köppen map. CRU TS V.4.02 provides a gridded time-series  
204 dataset based on observations from more than 4,000 sites over land.

205

-----

206

**Place Table 1**

207

-----

208 3.2 Köppen–Geiger climate classification

209 We used the Köppen–Geiger climate classification (Peel et al., 2007) to divide China  
210 into five climatic categories: tropical (A), arid (B), temperate (C), continental (D), and  
211 alpine (E) (Table S1). Given that the annual shifts in these climate zones may produce  
212 unrelated trends in the calculated results prior to the climate zoning analysis, we first  
213 applied the 5-year running mean to eliminate biases in climate variability (Mahlstein  
214 et al., 2013). Then, we determined the cumulative percentage of area change of all  
215 climatic zones during 1982–2012 relative to the spatial distribution in the first year  
216 (1982) (Huang et al., 2020). As each grid was assigned an initial climate category,  
217 altered grids were included if they shifted to a new climate type. Percentage area of  
218 specific climate was based on the number of grids of different climate types. To  
219 validate the applicability of our results, we compared the maps over the period 1982–

220 2012 to the map generated by the Climatic Research Unit (CRU) monthly temperature  
221 and precipitation (Figure S1-2).

### 222 3.3 Statistical analysis

223 One of the widely used non-parametric trend tests is the Mann–Kendall trend test  
224 (Text S1) (Mann, 1945; Kendall, 1975), which has been widely used to assess the  
225 significance of trends in meteorological time series. The null hypothesis in the Mann-  
226 Kendall test is that the data are independent and randomly ordered. The results  
227 elucidate the magnitude of the correlation and the direction of the relationship. The  
228 value of the coefficient ranges from 1 to  $-1$ , indicating a positive correlation and a  
229 negative correlation, respectively. Furthermore, we assume that the data are normally  
230 distributed. The null hypothesis states that the population correlation coefficient is  
231 equal to zero, which indicates that there is no linear correlation between the  
232 environmental variables. An alternative hypothesis was that it is not equal to zero.  
233 The t-test was used to determine whether the correlation coefficient was significantly  
234 different from zero, indicating an association between the two variables.

### 235 3.4 Sensitivity analysis

236 We conducted a sensitivity analysis to evaluate the evolution of climate zones in  
237 response to temperature and precipitation. First, we separately maintained each  
238 monthly temperature or precipitation at the same value as the initial year (1982) to  
239 compute the simulated percentage area of each climate zone. Second, we compared  
240 the experimental results with the observed percentage area of each zone to identify the

241 relative influence of the two climatic factors (e.g., either temperature or precipitation).  
242 Lastly, we utilised the coefficient of determination ( $r^2$ ) and significance ( $p$ ) value to  
243 determine the sensitivity of each climate zone to temperature and precipitation.

## 244 **4 Results**

### 245 4.1 Spatiotemporal variability of temperature, precipitation, and vegetation

246 We observed that the linear trends of annual temperature and precipitation featured  
247 clear spatial characteristics during 1982–2012 (Figure 2a-b). The highest rates of  
248 temperature rise were located in the Qinghai–Tibet Plateau (0.07 °C/y), East Inner  
249 Mongolia (0.05 °C/y), and the lower reaches of the Yangtze River (0.05 °C/y), while  
250 negative trends were most prominent in Northeast China (-0.01 °C/y). Negative trends  
251 in precipitation were predominantly observed in the middle and lower reaches of the  
252 Yangtze River (-25.2 mm/y), the Yunnan–Guizhou Plateau (-17.2 mm/y), and the  
253 Northeast Plain (-15.3 mm/y). Meanwhile, large increases in precipitation were  
254 observed in Northwest China, such as the Tianshan mountain region (6.3 mm/y) and  
255 the Qinghai–Tibet Plateau (9.4 mm/y).

256 In addition, we observed that the correlation between temperature and precipitation  
257 and NDVI between 1982 and 2012 has obvious regional characteristics. Overall, the  
258 temperature change ( $p < 0.05$ , MK) has a greater impact on vegetation growth than  
259 precipitation nationwide, especially in southern China and the Qinghai-Tibetan  
260 Plateau (Figure 2c), where NDVI is more sensitive to temperature changes. However,

261 NDVI in eastern Inner Mongolia and Tianshan area is more sensitive to precipitation  
262 decrease, with a significance level of 0.05 (t-test).

263 The spatiotemporal changes in temperature and precipitation will alter the regional  
264 climate zonation based on the Köppen–Geiger climate classification, and different  
265 climatic zones are likely to have varying sensitivities to the changes. For example, the  
266 rapid temperature increase in the Qinghai–Tibet Plateau is likely to result in a  
267 shrinking of the alpine climate zone and an expansion of the continental climate zone,  
268 triggering a rapid response to vegetation changes, including types and distribution.  
269 Furthermore, the observed decrease in precipitation in the Northeast Plain is likely to  
270 lead to the expansion of arid climate zones.

271 -----

272 **Place Figure 2**

273 -----

#### 274 4.2 Spatiotemporal variability in the climate zone

275 Figure 3 illustrates the spatial distribution of China’s climate zones in 1982, 1990,  
276 2000, and 2010. Table 2 compares the 1990, 2000, and 2010 results relative to the  
277 baseline time (1982). The comparisons of 1982 to 1990 and 2000 to 2010 show that  
278 the percentage areas of arid zones are, respectively, reduced by -1.1% and -1.74%, but  
279 expanded from 1990 to 2000. In space, the largest changes in the percentage area of

280 arid zones were concentrated on the North China Plain and the Northeast Plains.

281 Many areas alternated between the continental and arid climates—particularly in the

282 northeast—in response to changes in precipitation, such as the marked precipitation

283 reduction from 1990 to 2005 (Figure 2b). The percentage area of the temperate zone

284 has expanded since 1982, with the highest increase (1.34%) observed from 1982 to

285 1990. Spatially, these changes occurred at the northern boundary of the temperate

286 zone. The boundary between the Qinling Mountain and the Huaihe River Line shifted

287 towards the north between 1982 and 1990, and gradually back towards the south

288 thereafter. The temporal trends in the percentage area of the continental zone are

289 directly opposite to the trend in the arid zone, which expanded by 0.2% and 1.95%

290 from 1982 to 1990, and from 2000 to 2010, respectively, and reduced by -3.72% from

291 1990 to 2000. The total percentage area of the alpine zone has decreased consistently

292 since 1982. Spatially, these changes occurred at the boundary between the alpine and

293 continental zones. The areal expansion of the temperate zone resulted in the alpine

294 zone in the Qinghai–Tibet Plateau shrinking, which has been predominantly replaced

295 by the continental zone. In general, we observed clear fluctuations in the percentage

296 area of arid, temperate, and continental zones, and a continued decrease in the

297 percentage area of alpine zone since 1982.

298

-----

299

**Place Figure 3**

300

-----

301

-----

302

**Place Table 2**

303

-----

304 Figure 4 indicates that the cumulative percentage of area change in all climate zones  
305 significantly increased from 12.08% to 18.98% at a rate of 0.204%/y from 1983 to  
306 2012 at a significance level of 0.05 (MK). However, we observed differences in the  
307 percentage area change between each climate zone from 1982 to 2012 (Figure 5). In  
308 general, the arid and continental zones expanded at rates of 0.004%/y and 0.12%/y,  
309 respectively, while the percentage areas of temperate and alpine zones decreased by -  
310 0.05%/y and -0.07%/y at a significance level of 0.05, respectively. Moreover, we  
311 detected a signal over each climate zone in 2005, where the percentage areas of the  
312 arid and temperate zones evidently decreased from 34.46% to 25.26% and 22.8% to  
313 22.52%, respectively. The area of the continental and alpine zones increased from  
314 26.01% to 34.1% and 16.58% to 17.32%, respectively. These change trends around  
315 2005 should be attributed to the differential response of specific climate zones to  
316 notable changes in temperature and precipitation.

317

-----

318

**Place Figure 4**



319

-----

320

-----

321

**Place Figure 5**

322

-----

### 323 4.3 Climate zone sensitivity to driving forces

324 Figure 6 and Table 3 show the linear fitting results of the sensitivity experiments  
325 between observed and simulated percentage areas for specific climate zones in  
326 different scenarios during 1982–2012. Where temperature is held constant, the  
327 simulated change in the percentage area approximates the observed changes with  $r^2$  of  
328 0.855 and 0.815 ( $p < 0.01$ , t-test) in arid and continental zones, respectively. In this  
329 case, the linear fitting coefficients between the simulated and observed changes are  
330 0.646 and 0.514 ( $p < 0.01$ , t-test) in the temperate and alpine zones, respectively. On  
331 the contrary, where precipitation is held constant, the linear fitting coefficients of  
332 simulated to observed changes are 0.473 and 0.753 ( $p < 0.01$ , t-test) in arid and  
333 continental zones, respectively. However, the correlation between the observed and  
334 simulated percentage area was stronger with temperature change, with  $r^2$  values of  
335 0.98 and 0.968 ( $p < 0.01$ , t-test) in the temperate and alpine zones, respectively. In  
336 general, through sensitivity analysis, precipitation seems to be the main driver in the  
337 dynamics of arid and continental zones, while temperature dominates the area change

338 of temperate and alpine zones. However, considering the nature of the Köppen  
339 scheme, temperature and precipitation essentially determine the changes in different  
340 climate zones. Therefore, we cannot ignore the important role of non-dominant  
341 factors in their respective climate zones. Particularly, in the continental zone the  
342 fitting coefficients between the simulated and observed changes in different scenarios  
343 are relatively close, with  $r^2$  values of 0.815 and 0.753, respectively, indicating that  
344 temperature change also plays an important role in the change process in specific  
345 climate zone.

346

-----

347

**Place Figure 6**

348

-----

349

-----

350

**Place Table 3**

351

-----

352 4.4 Response of vegetation to climate zone and links to surface soil water content and  
353 albedo

354 Figure 7 shows the trends in the annual SW content, NDVI, albedo, and the  
355 correlation between albedo and NDVI for the period 1982–2012. Spatial changes in  
356 NDVI are related to surface moisture and albedo. We observed a decrease in surface  
357 SW content in the Northeast Mountains area and South China (Figure 7a). In contrast,  
358 we observed a gradual increase in soil moisture content in the middle and west of  
359 Tibet, the Northeast plain, and the Huaihe River Basin. We observed an increase in  
360 NDVI in the Northeast Plain, Huaihe River Basin, and the Tianshan Mountains  
361 (Figure 7b), and a decrease in NDVI in the Northeast, Yangtze River, Pearl River, and  
362 Yunnan–Guizhou Plateau. The albedo trends of the middle and lower reaches of the  
363 Yangtze River Basin, the Northeast Mountains, Southern China, and the Western  
364 border mountains are more pronounced than elsewhere (Figure 7c). Figure 7d  
365 illustrates the correlation between the NDVI and albedo. Albedo and NDVI were  
366 positively correlated in Central and Western China, particularly in the Northeast plain,  
367 the Yarlung Zangbo River Basin, and in Eastern Inner Mongolia.

368

-----

369

**Place Figure 7**

370

-----

371 Figure 8 depicts the relationship between the percentage area of each climate zone  
372 and their dominant driving factors (precipitation or temperature based on the  
373 sensitivity experiments), NDVI, and SW anomalies during 1982–2012. In general,  
374 changes in the percentage area of each climate zone are clearly related to the  
375 dominant driving factor, while changes in NDVI are influenced directly by SW  
376 content affected by the climate zone.

377 The percentage area of the arid zone increased slightly prior to 2005, which was  
378 consistent with changes in precipitation (Figure 8a). In contrast, the percentage area of  
379 arid zones decreased after 2005, which is opposite to the observed precipitation trend.  
380 With the rapid increase in precipitation, the percentage area of the arid zone and SW  
381 tended to decrease. Temperature was the dominant control on the percentage area of  
382 temperate zones. After 2005, the percentage area reduced from 27.91% to 26.52% in  
383 response to a temperature decrease from 16.71 °C to 16.16 °C. Since 2005, the area  
384 reduction of temperate climate has been concentrated on the North China Plain, where  
385 precipitation and SW have increased rapidly. Due to the decrease in coverage of  
386 temperate zones and the decrease in precipitation in the Yangtze River area, NDVI  
387 decreased from 0.646 to 0.524 since 2005. The percentage area of the continental  
388 zone increased from 23.36% to 27.20% in response to an increase in precipitation  
389 from 472 mm to 572 mm, as the evolution of the continental zone is more sensitive to  
390 changes in precipitation than changes in temperature. With the decrease in  
391 precipitation and SW before 2005, the disappearing area was mainly in the Northeast

392 Plain, and the overall NDVI of the continental zone increased due to the increase in  
393 the proportion of forest area. Since 2005, due to the rapid increase in precipitation, the  
394 percentage area has also increased rapidly, particularly in the Northeast Plain and  
395 Qinghai-Tibet Plateau, which decreased the overall SW and NDVI in the continental  
396 zone. The percentage area of the alpine zone was negatively correlated with changes  
397 in temperature and SW. Prior to 2005, the percentage area decreased from 21.9% to  
398 20.9% in response to increasing temperature from  $-4.8\text{ }^{\circ}\text{C}$  to  $-3.7\text{ }^{\circ}\text{C}$ . However, the  
399 percentage area expanded from 20.9% to 21.2% and the NDVI increased from 0.371  
400 to 0.379 since 2005 in response to a temperature change from  $-3.7\text{ }^{\circ}\text{C}$  to  $-4.3\text{ }^{\circ}\text{C}$ .  
401 Since 2005, the emerging area of the alpine zone has been concentrated between the  
402 alpine zone and the continental zone where the vegetation status is usually more  
403 productive than of that in the alpine zone.

404 -----

405 **Place Figure 8**

406 -----

407 Figure 9 shows the response of annual NDVI variability to albedo from 1982 to 2012.  
408 In general, there are evident differences between NDVI and albedo in different  
409 climate zones. For temperate and alpine climate zones, we found that the changes in  
410 NDVI were significantly correlated to albedo ( $p < 0.05$ , t-test) during 1982–2012, in  
411 which the higher NDVI basically corresponds to lower albedo. However, the

412 relationship between albedo and NDVI is more complex in arid and continental  
413 climates, particularly during 1995–2005.

414 The NDVI correlated significantly with albedo ( $r = -0.82, p < 0.01$ ) in the temperate  
415 zone (Figure 9b). Surface SW content after 2005 resulted in a rapid decrease of NDVI  
416 from 0.32 to 0.28, while the albedo increased from 0.17 to 0.18. NDVI also correlated  
417 significantly with albedo during 1982–2012 ( $r = -0.476, p < 0.05$ ) in the alpine zone.

418 Changes in temperature and surface SW since 2005 resulted in an increase in NDVI  
419 and a decrease in albedo from 0.187 to 0.185.

420 In the arid and continental climate zones, the NDVI variability during 1982–1995 and  
421 2005–2012 was negatively correlated with albedo, while NDVI variability positively  
422 correlated with albedo during the period 1995–2005. In particular, the observed  
423 changes in 1995–2005 predominantly occurred in the Northeast Plain, where  
424 precipitation had reduced and caused an increase in albedo. Precipitation is the  
425 dominant control on the evolution of arid and continental climate zones, as changes in  
426 precipitation caused notable shifts in the two climate types. Cultivated vegetation is  
427 predominantly distributed in the Northeast Plain, according to the Chinese vegetation  
428 atlas (2000). The NDVI increased from 1995 to 2005 in arid climate zones, as the  
429 NDVI in the changed area was clearly higher than in low shrubland, meadows, and  
430 desert regions. Furthermore, decreasing precipitation in continental climate zones had  
431 reduced NDVI from 0.45. to 0.43, while albedo decreased from 0.183 to 0.181 from  
432 1995 to 2005.

433

-----

434

**Place Figure 9**

435

-----

436 Figure 10 further highlights the observed differences in NDVI, albedo, and SW trends  
437 of specific climate zones. SW content and NDVI predominantly increased and the  
438 albedo decreased during the vegetation growing periods. The SW content in the arid  
439 zone significantly decreased from February to April at rates of  $-0.4 \times 10^{-3} \text{ m}^3 \text{ m}^{-3}/\text{y}$  to  
440  $-0.7 \times 10^{-3} \text{ m}^3 \text{ m}^{-3}/\text{y}$ . We also observed significant decreases in February, March,  
441 April, and September (continental zones). A significant increasing trend in June and a  
442 decreasing trend in March and September were detected in the alpine climate zone.  
443 The significant decrease in NDVI occurred in November and December during the  
444 non-vegetation growing period (continental zones). Furthermore, in the arid and  
445 alpine zones, the monthly trends of albedo increased, while predominant trends in  
446 temperate and continental climates decreased. More importantly, weak changes in  
447 albedo accompanied the strong trends in NDVI and SW content during the vegetation  
448 growing periods.

449

-----

450

**Place Figure 10**

451

-----

## 452 **5 Discussion**

453 The spatial scales at which climate changes are measured are extremely important,  
454 since the response mechanism may change as the scale changes (Aalto et al., 2018;  
455 Chen et al., 2017; Järvi et al., 2019; Wu, 2004). On the one hand, our results reveal  
456 that major climate zones respond differently to changes in temperature and  
457 precipitation, indicating that arid and continental zones are more sensitive to  
458 precipitation, while temperate and alpine zones are more responsive to temperature. It  
459 should be noted that global universal climate change laws are not necessarily  
460 applicable to regional-scale climate change. Recent studies (Burrows et al., 2011; Lu  
461 et al., 2019; Mahlstein et al., 2013; Sunday et al., 2011) have shown that global  
462 warming determines the dynamics of global climate zones. However, our results  
463 demonstrate that it does not necessarily determine the dynamics in regional climate  
464 zones. On the other hand, we must consider the climate zone change at different  
465 spatial resolutions, as the statistical results may change as the possible uncertainty of  
466 different spatial resolutions. In this study, we selected regional high-density  
467 meteorological data with a resolution of  $0.5^\circ$  to explore changes in regional climate  
468 zones. This is because the application of relatively coarse spatial resolution may limit  
469 the effectiveness of climatic assessments and potential ecological impacts, particularly  
470 when it is insufficient to describe small-scale features such as in some high mountain  
471 areas (Beck et al., 2018; Rohli et al., 2015b). In view of this, climate change research



472 must fully consider the selection of a suitable spatial research scale and resolution  
473 because this will help us understand the climate itself (Guan et al., 2020).

474 In addition, our results demonstrate that overall changes in the percentage area of each  
475 climate zone were related to surface SW content, NDVI, and albedo in regions of high  
476 (temperate zones) and low (alpine zones) vegetation coverage. Since climate zones  
477 are considered a substitute for vegetation distribution (Rohli et al., 2015; Wang &  
478 Overland, 2004), regional climate zones may show some similarities in the surface  
479 biophysical properties of land cover. Changes in land cover influence radiative  
480 forcing and have been shown to directly affect regional energy balances (Abera et al.,  
481 2019a; Lee Et al., 2011; Li et al., 2015). Similar to shifts in land cover, when climate  
482 zones expand or shrink in response to changes in regional temperature or  
483 precipitation, these changes can also affect the greening or browning of regional  
484 vegetation (Chen et al., 2019), altering regional surface roughness, albedo,  
485 evaporation, and net radiation partitioning. However, it is not easy to fully elucidate  
486 the interactive mechanisms and feedbacks related to the regional energy balance  
487 based on shifts of climate zones, such as at the pixel level (Armstrong et al., 2016;  
488 Gerken et al., 2018; Stark et al., 2016). This is due to the lack of observational data on  
489 key climatic and biophysical variables, particularly in remote regions. Furthermore,  
490 according to the empirical nature of the Köppen classification scheme, the fluctuating  
491 climatic zone is significantly different from the surface reference for vegetation cover

492 with multi-year persistence. Despite these limitations, the study still effectively sheds  
493 light on the impact of shifting climate zones on the surface biophysical characteristics.

494 Our results also indicate inconsistencies in the correlations between climate zone  
495 shifts, NDVI and albedo in arid and continental climate zones. From 1995 to 2005,  
496 the precipitation-controlled shifts between arid and continental zones were mainly  
497 concentrated in the Northeast Plain. Due to the decrease in precipitation (Figure 2b),  
498 the continental zone in the Northeast Plain was replaced by arid zones. However,  
499 there was no obvious change in the type and distribution of vegetation, which may not  
500 only be due to human activities but also likely affected by the inertness of modern  
501 ecosystems to climate change (Scheffer et al., 2001). On the one hand, human  
502 activities such as large-scale agricultural reclamation and irrigation (Piao et al., 2003;  
503 Zhu et al., 2013) could change regional soil properties (e.g., moisture, pH, organic  
504 matter, nitrogen, and microorganisms) to affect the succession of vegetation types  
505 (Jiang et al., 2020), further influencing the biophysical characteristics of vegetation  
506 types. On the other hand, the threshold range of precipitation in response to different  
507 vegetation types could be more stable than that of the precipitation range of the  
508 Köppen arid climate (Mahlstein et al., 2013; Peel et al., 2007). Zhao et al. (2015)  
509 indicated that a threshold effect may exist in the vegetation response to climate  
510 change in many ecosystems. Although it is difficult to distinguish the different effects  
511 quantitatively, internal and external feedback jointly promote the stability of regional  
512 ecosystems and vegetation types.

## 513 **6 Conclusion**

514 In this study, we investigated the vegetation response to shifting climate zones and its  
515 potential impacts on albedo and SW content in China. As the substantial changes in  
516 temperature and precipitation across time and space, we detected significant shifts in  
517 climate zonation on a nationwide level. From 1983 to 2012, the cumulative  
518 percentage of area change in all climate zones significantly increased from 12.08% to  
519 18.98% at an annual growth rate of 0.204% ( $p < 0.05$ , MK). The percentage areas of  
520 arid and continental zones expanded at rates of 0.004%/y and 0.12%/y, respectively,  
521 while the temperate and alpine zones decreased by -0.05%/y and -0.07%/y,  
522 respectively. Sensitivity results in the different simulated cases suggest that the  
523 temperature and precipitation impact in specific climate zones are different.  
524 Specifically, temperature is the dominant control on the evolution of temperate and  
525 alpine zones with  $r^2$  of 0.98 and 0.968 between simulated and observed changes,  
526 respectively, while precipitation is the dominant control on the evolution of arid and  
527 continental zones with  $r^2$  of 0.856 and 0.815, respectively. Vegetation substantially  
528 responds to shifting climate zones with impact on surface biophysical characteristics.  
529 Specifically, a pronounced albedo and NDVI feedback response was detected in  
530 temperate and alpine zones with a 0.05 significance level. However, inconsistent  
531 feedbacks of NDVI to albedo were also reported in arid and continental climates,  
532 particularly during 1995-2005. Furthermore, recent climate warming has influenced

533 the seasonal trends in vegetation activity. The SW content and NDVI predominantly  
534 increased and the albedo decreased during the vegetation growing periods.

535 In general, the redistribution of vegetation has emerged as one of the most  
536 pronounced biological responses to climate change. Considering that the vegetation  
537 distribution represents an expression of ‘visible climate’, the rapid increase or  
538 decrease of climate-suitable areas will alter their distributional ranges and seasonal  
539 activities to maintain their niche, especially as the global temperature may increase by  
540 at least 1.5°C in the near future. If the speed of vegetation species tracks or adaptations  
541 to climate conditions cannot reach the rate of climate change, it may lead to the  
542 disaggregation of vegetation species assemblages, and the spatial distribution of  
543 original vegetation will be gradually replaced by novelty vegetation, in which regional  
544 surface biophysical characteristics and radiative mechanisms will inevitably change,  
545 especially in the event of accelerated warming in the future. Moreover, future relevant  
546 analysis may be useful in a wide range of environmental topics, especially with the  
547 advent of continuous high-quality and high-resolution data products, which will  
548 improve our ability to describe climate types in areas of sharp climatic gradients (e.g.  
549 mountainous areas of the Qinghai-Tibet Plateau).

## 550 **Acknowledgments**

551 We appreciate National Meteorological Information Center (NMIC) of the China and  
552 the Global Inventory Monitoring and Modeling System (GIMMS) project as well as

553 European Centre for Medium-Range Weather Forecasts (ECMWF) to provide the  
554 public observed and reanalyzed datasets. This research is supported by the Strategic  
555 Priority Research Program of Chinese Academy of Sciences (XDA20040301), the  
556 National Natural Science Foundation of China (41890824), and the Fundamental  
557 Research Funds for the Central Universities. The data archiving in this study has  
558 archived at the Mendeley repository (<https://data.mendeley.com/>). Furthermore, we  
559 would like to thank anonymous reviewers for their useful comments on the  
560 manuscript.

561

562 **Reference:**

563 Aalto, J., Karjalainen, O., Hjort, J., Luoto, M., 2018. Statistical Forecasting of Current  
564 and Future Circum-Arctic Ground Temperatures and Active Layer Thickness.

565 *Geophys. Res. Lett.* 45, 4889–4898. <https://doi.org/10.1029/2018GL078007>

566 Abera, T.A., Heiskanen, J., Pellikka, P., Rautiainen, M., Maeda, E.E., 2019.

567 Clarifying the role of radiative mechanisms in the spatio-temporal changes of

568 land surface temperature across the Horn of Africa. *Remote Sens. Environ.* 221,

569 210–224. <https://doi.org/10.1016/j.rse.2018.11.024>

570 Armstrong, E., Valdes, P., House, J., Singarayer, J., 2016. The role of CO<sub>2</sub> and

571 dynamic vegetation on the impact of temperate land-use change in the HadCM3

572 coupled climate model. *Earth Interact.* 20. <https://doi.org/10.1175/EI-D-15->

573 0036.1

574 Beck, H.E., Zimmermann, N.E., McVicar, T.R., Vergopolan, N., Berg, A., Wood,  
575 E.F., 2018. Present and future köppen-geiger climate classification maps at 1-km  
576 resolution. *Sci. Data* 5, 1–12. <https://doi.org/10.1038/sdata.2018.214>

577 Burrows, M.T., Schoeman, D.S., Buckley, L.B., Moore, P., Poloczanska, E.S.,  
578 Brander, K.M., Brown, C., Bruno, J.F., Duarte, C.M., Halpern, B.S., Holding, J.,  
579 Kappel, C. V., Kiessling, W., O'Connor, M.I., Pandolfi, J.M., Parmesan, C.,  
580 Schwing, F.B., Sydeman, W.J., Richardson, A.J., 2011. The pace of shifting  
581 climate in marine and terrestrial ecosystems. *Science* (80-. ). 334, 652–655.  
582 <https://doi.org/10.1126/science.1210288>

583 Carey, M., Molden, O.C., Rasmussen, M.B., Jackson, M., Nolin, A.W., Mark, B.G.,  
584 2017. Impacts of Glacier Recession and Declining Meltwater on Mountain  
585 Societies. *Ann. Am. Assoc. Geogr.* 107, 350–359.  
586 <https://doi.org/10.1080/24694452.2016.1243039>

587 Chen, C., Park, T., Wang, X., Piao, S., Xu, B., Chaturvedi, R.K., Fuchs, R., Brovkin,  
588 V., Ciais, P., Fensholt, R., Tømmervik, H., Bala, G., Zhu, Z., Nemani, R.R.,  
589 Myneni, R.B., 2019. China and India lead in greening of the world through land-  
590 use management. *Nat. Sustain.* 2, 122–129. [https://doi.org/10.1038/s41893-019-](https://doi.org/10.1038/s41893-019-0220-7)  
591 [0220-7](https://doi.org/10.1038/s41893-019-0220-7)

592 Chen, T., Zhang, H., Chen, X., Hagan, D.F., Wang, G., Gao, Z., Shi, T., 2017. Robust  
593 drying and wetting trends found in regions over China based on Köppen climate  
594 classifications. *J. Geophys. Res.* 122, 4228–4237.  
595 <https://doi.org/10.1002/2016JD026168>

596 Dee, D.P., Uppala, S.M., Simmons, A.J., Berrisford, P., Poli, P., Kobayashi, S.,  
597 Andrae, U., Balmaseda, M.A., Balsamo, G., Bauer, P., Bechtold, P., Beljaars,  
598 A.C.M., van de Berg, L., Bidlot, J., Bormann, N., Delsol, C., Dragani, R.,  
599 Fuentes, M., Geer, A.J., Haimberger, L., Healy, S.B., Hersbach, H., Hólm, E. V.,  
600 Isaksen, L., Kållberg, P., Köhler, M., Matricardi, M., McNally, A.P., Monge-  
601 Sanz, B.M., Morcrette, J.J., Park, B.K., Peubey, C., de Rosnay, P., Tavolato, C.,  
602 Thépaut, J.N., Vitart, F., 2011. The ERA-Interim reanalysis: Configuration and  
603 performance of the data assimilation system. *Q. J. R. Meteorol. Soc.* 137, 553–  
604 597. <https://doi.org/10.1002/qj.828>

605 Editorial Board for Chinese Vegetation Map, Chinese Academy of Sciences.  
606 Vegetation Atlas of China (1:100000). Beijing: Science Press, 2001: 129-132.

607 Engelbrecht, C.J., Engelbrecht, F.A., 2016. Shifts in Köppen-Geiger climate zones  
608 over southern Africa in relation to key global temperature goals. *Theor. Appl.*  
609 *Climatol.* 123, 247–261. <https://doi.org/10.1007/s00704-014-1354-1>

610 Erasmi, S., Dulamsuren, C., Hauck, M., Klinge, M., Karger, D.N., 2017. Climate  
611 effects on the vitality of boreal forests at the treeline in different ecozones of  
612 Mongolia. *Biogeosciences Discuss.* 1–25. <https://doi.org/10.5194/bg-2017-220>

613 Erb, K.H., Luysaert, S., Meyfroidt, P., Pongratz, J., Don, A., Kloster, S., Kuemmerle,  
614 T., Fetzel, T., Fuchs, R., Herold, M., Haberl, H., Jones, C.D., Marín-Spiotta, E.,  
615 McCallum, I., Robertson, E., Seufert, V., Fritz, S., Valade, A., Wiltshire, A.,  
616 Dolman, A.J., 2017. Land management: data availability and process  
617 understanding for global change studies, *Global Change Biology.*

618 <https://doi.org/10.3945/ajcn.116.130518>

619 Fan, Y., van den Dool, H., 2008. A global monthly land surface air temperature  
620 analysis for 1948-present. *J. Geophys. Res. Atmos.* 113, 1–18.  
621 <https://doi.org/10.1029/2007JD008470>

622 Fang, J., Piao, S., He, J., Ma, W., 2004. Increasing terrestrial vegetation activity in  
623 China, 1982-1999. *Sci. China, Ser. C Life Sci.* 47, 229–240.  
624 <https://doi.org/10.1360/03yc0068>

625 Farmer, G.T., Cook, J., 2013. Climate change science: A modern synthesis: Volume 1  
626 - The physical climate. *Clim. Chang. Sci. A Mod. Synth. Vol. 1 - Phys. Clim.* 1,  
627 1–564. <https://doi.org/10.1007/978-94-007-5757-8>

628 Flemming, J., Huijnen, V., Arteta, J., Bechtold, P., Beljaars, A., Blechschmidt, A.M.,  
629 Diamantakis, M., Engelen, R.J., Gaudel, A., Inness, A., Jones, L., Josse, B.,  
630 Katragkou, E., Marecal, V., Peuch, V.H., Richter, A., Schultz, M.G., Stein, O.,  
631 Tsikerdekis, A., 2015. Tropospheric chemistry in the integrated forecasting  
632 system of ECMWF. *Geosci. Model Dev.* 8, 975–1003.  
633 <https://doi.org/10.5194/gmd-8-975-2015>

634 Garcia, R.A., Cabeza, M., Rahbek, C., Araújo, M.B., 2014. Multiple dimensions of  
635 climate change and their implications for biodiversity. *Science* (80-. ). 344.  
636 <https://doi.org/10.1126/science.1247579>

637 Gerken, T., Ruddell, B.L., Fuentes, J.D., Araújo, A., Brunzell, N.A., Maia, J., Manzi,  
638 A., Mercer, J., dos Santos, R.N., von Randow, C., Stoy, P.C., 2018. Investigating  
639 the mechanisms responsible for the lack of surface energy balance closure in a



640 central Amazonian tropical rainforest. *Agric. For. Meteorol.* 255, 92–103.  
641 <https://doi.org/10.1016/j.agrformet.2017.03.023>

642 Gottfried, M., Pauli, H., Futschik, A., Akhalkatsi, M., Barančok, P., Benito Alonso,  
643 J.L., Coldea, G., Dick, J., Erschbamer, B., Fernández Calzado, M.R., Kazakis,  
644 G., Krajčí, J., Larsson, P., Mallaun, M., Michelsen, O., Moiseev, D., Moiseev, P.,  
645 Molau, U., Merzouki, A., Nagy, L., Nakhutsrishvili, G., Pedersen, B., Pelino, G.,  
646 Puscas, M., Rossi, G., Stanisci, A., Theurillat, J.-P., Tomaselli, M., Villar, L.,  
647 Vittoz, P., Vogiatzakis, I., Grabherr, G., 2012. Continent-wide response of  
648 mountain vegetation to climate change. *Nat. Clim. Chang.* 2, 111–115.  
649 <https://doi.org/10.1038/nclimate1329>

650 Guan, Y., Lu, H., He, L., Adhikari, H., Pellikka, P., Maeda, E., Heiskanen, J., 2020.  
651 Intensification of the Dispersion of the Global Climatic Landscape and its  
652 Potential as a New Climate Change Indicator. *Environ. Res. Lett.* 10, in press.

653 Guetter, P.J., Kutzbach, J.E., 1990. A modified Köppen classification applied to  
654 model simulations of glacial and interglacial climates. *Clim. Change* 16, 193–  
655 215. <https://doi.org/10.1007/BF00134657>

656 Harris, I., Jones, P.D., Osborn, T.J., Lister, D.H., 2014. Updated high-resolution grids  
657 of monthly climatic observations - the CRU TS3.10 Dataset. *Int. J. Climatol.* 34,  
658 623–642. <https://doi.org/10.1002/joc.3711>

659 Harris, R.M.B., Remenyi, T.A., Williamson, G.J., Bindoff, N.L., Bowman, D.M.J.S.,  
660 2016. Climate–vegetation–fire interactions and feedbacks: trivial detail or major  
661 barrier to projecting the future of the Earth system? *Wiley Interdiscip. Rev.*

662 Clim. Chang. 7, 910–931. <https://doi.org/10.1002/wcc.428>

663 Helmens, K.F., Katrantsiotis, C., Sakari Salonen, J., Shala, S., Bos, J.A.A., Engels, S.,  
664 Kuosmanen, N., Luoto, T.P., Väiliranta, M., Luoto, M., Ojala, A., Risberg, J.,  
665 Weckström, J., 2018. Warm summers and rich biotic communities during N-  
666 Hemisphere deglaciation. *Glob. Planet. Change* 167, 61–73.  
667 <https://doi.org/10.1016/j.gloplacha.2018.05.004>

668 Huang, J., Yu, H., Guan, X., Wang, G., Guo, R., 2016. Accelerated dryland expansion  
669 under climate change. *Nat. Clim. Chang.* 6, 166–171.  
670 <https://doi.org/10.1038/nclimate2837>

671 Huang, X., Ma, L., Liu, T., Sun, B., Zhou, Y., Chen, Y., Qiao, Z., 2020. Spatial  
672 Variability in Years of Abrupt Seasonal Temperature Changes and Warming  
673 (Cooling) Hiatuses in China from 1951–2018 and the Variation Trends before  
674 and after These Years. *Atmosphere (Basel)*. 11, 82.  
675 <https://doi.org/10.3390/atmos11010082>

676 Järvi, L., Havu, M., Ward, H.C., Bellucco, V., McFadden, J.P., Toivonen, T.,  
677 Heikinheimo, V., Kolari, P., Riikonen, A., Grimmond, C.S.B., 2019. Spatial  
678 Modeling of Local-Scale Biogenic and Anthropogenic Carbon Dioxide  
679 Emissions in Helsinki. *J. Geophys. Res. Atmos.* 8363–8384.  
680 <https://doi.org/10.1029/2018jd029576>

681 Jiang, Y., Guo, J., Peng, Q., Guan, Y., Zhang, Y., Zhang, R., 2020. The effects of  
682 climate factors and human activities on net primary productivity in Xinjiang. *Int.*  
683 *J. Biometeorol.* <https://doi.org/10.1007/s00484-020-01866-4>

684 Kendall MG. 1975. Rank Correlation Methods. Griffin: London.

685 Lee, X., Goulden, M.L., Hollinger, D.Y., Barr, A., Black, T.A., Bohrer, G., Bracho,  
686 R., Drake, B., Goldstein, A., Gu, L., Katul, G., Kolb, T., Law, B.E., Margolis,  
687 H., Meyers, T., Monson, R., Munger, W., Oren, R., Paw U, K.T., Richardson,  
688 A.D., Schmid, H.P., Staebler, R., Wofsy, S., Zhao, L., 2011. Observed increase  
689 in local cooling effect of deforestation at higher latitudes. *Nature* 479, 384–387.  
690 <https://doi.org/10.1038/nature10588>

691 Li, Q., Ma, M., Wu, X., Yang, H., 2018. Snow Cover and Vegetation-Induced  
692 Decrease in Global Albedo From 2002 to 2016. *J. Geophys. Res. Atmos.* 123,  
693 124–138. <https://doi.org/10.1002/2017JD027010>

694 Li, Y., Zhao, M., Motesharrei, S., Mu, Q., Kalnay, E., Li, S., 2015. Local cooling and  
695 warming effects of forests based on satellite observations. *Nat. Commun.* 6.  
696 <https://doi.org/10.1038/ncomms7603>

697 Lu, H., Guan, Y., He, L., Adhikari, H., Pellikka, P., Heiskanen, J., Maeda, E., 2019.  
698 Patch aggregation trends of the global climate landscape under future global  
699 warming scenario. *Int. J. Climatol.* <https://doi.org/10.1002/joc.6358>

700 Mahlstein, I., Daniel, J.S., Solomon, S., 2013. Pace of shifts in climate regions  
701 increases with global temperature. *Nat. Clim. Chang.* 3, 739–743.  
702 <https://doi.org/10.1038/nclimate1876>

703 Mann, H. B. (1945). Nonparametric tests against trend. *Econometrica: Journal of the*  
704 *Econometric Society* , 245-259.

705 Martin-Benito, D., Pederson, N., 2015. Convergence in drought stress, but a

706 divergence of climatic drivers across a latitudinal gradient in a temperate  
707 broadleaf forest. *J. Biogeogr.* 42, 925–937. <https://doi.org/10.1111/jbi.12462>

708 McColl, K.A., Alemohammad, S.H., Akbar, R., Konings, A.G., Yueh, S., Entekhabi,  
709 D., 2017. The global distribution and dynamics of surface soil moisture. *Nat.*  
710 *Geosci.* 10, 100–104. <https://doi.org/10.1038/ngeo2868>

711 Park, S., 2010. IFS Documentation - Cy36r1: PART IV: PHYSICAL PROCESSES  
712 1–171.

713 Pauli, H., Gottfried, M., Dullinger, S., Abdaladze, O., Akhalkatsi, M., Alonso, J.L.B.,  
714 Coldea, G., Dick, J., Erschbamer, B., Calzado, R.F., Ghosn, D., Holten, J.I.,  
715 Kanka, R., Kazakis, G., Kollár, J., Larsson, P., Moiseev, P., Moiseev, D., Molau,  
716 U., Mesa, J.M., Nagy, L., Pelino, G., Puşcaş, M., Rossi, G., Stanisci, A.,  
717 Syverhuset, A.O., Theurillat, J.P., Tomaselli, M., Unterluggauer, P., Villar, L.,  
718 Vittoz, P., Grabherr, G., 2012. Recent plant diversity changes on Europe's  
719 mountain summits. *Science* (80-. ). <https://doi.org/10.1126/science.1219033>

720 Pearson, R.G., Phillips, S.J., Loranty, M.M., Beck, P.S.A., Damoulas, T., Knight, S.J.,  
721 Goetz, S.J., 2013. Shifts in Arctic vegetation and associated feedbacks under  
722 climate change. *Nat. Clim. Chang.* 3, 673–677.  
723 <https://doi.org/10.1038/nclimate1858>

724 Peel, M.C., Finlayson, B.L., McMahon, T.A., 2007. Updated world map of the  
725 Köppen-Geiger climate classification. *Hydrol. Earth Syst. Sci.* 11, 1633–1644.  
726 <https://doi.org/10.5194/hess-11-1633-2007>

727 Piao, S., Fang, J., Zhou, L., Guo, Q., Henderson, M., Ji, W., Li, Y., Tao, S., 2003.

728 Interannual variations of monthly and seasonal normalized difference vegetation  
729 index (NDVI) in China from 1982 to 1999. *J. Geophys. Res. D Atmos.* 108, 1–  
730 13. <https://doi.org/10.1029/2002jd002848>

731 Piao, S., Yin, G., Tan, J., Cheng, L., Huang, M., Li, Y., Liu, R., Mao, J., Myneni,  
732 R.B., Peng, S., Poulter, B., Shi, X., Xiao, Z., Zeng, N., Zeng, Z., Wang, Y.,  
733 2015. Detection and attribution of vegetation greening trend in China over the  
734 last 30 years. *Glob. Chang. Biol.* 21, 1601–1609.  
735 <https://doi.org/10.1111/gcb.12795>

736 Pinzon, J.E., Tucker, C.J., 2014. A non-stationary 1981–2012 AVHRR NDVI3g time  
737 series. *Remote Sens.* 6, 6929–6960. <https://doi.org/10.3390/rs6086929>

738 Pithan, F., Mauritsen, T., 2014. Arctic amplification dominated by temperature  
739 feedbacks in contemporary climate models. *Nat. Geosci.* 7, 181–184.  
740 <https://doi.org/10.1038/ngeo2071>

741 Ren, Z., Zhang, M., Wang, S., Qiang, F., Zhu, X., Dong, L., 2015. Changes in daily  
742 extreme precipitation events in South China from 1961 to 2011. *J. Geogr. Sci.*  
743 25, 58–68. <https://doi.org/10.1007/s11442-015-1153-3>

744 Richardson, A.D., Keenan, T.F., Migliavacca, M., Ryu, Y., Sonnentag, O., Toomey,  
745 M., 2013. Climate change, phenology, and phenological control of vegetation  
746 feedbacks to the climate system. *Agric. For. Meteorol.* 169, 156–173.  
747 <https://doi.org/10.1016/J.AGRFORMET.2012.09.012>

748 Rohli, R. V., Andrew Joyner, T., Reynolds, S.J., Shaw, C., Vázquez, J.R., 2015a.  
749 Globally Extended Kppen-Geiger climate classification and temporal shifts in

750 terrestrial climatic types. *Phys. Geogr.* 36, 142–157.  
751 <https://doi.org/10.1080/02723646.2015.1016382>

752 Rohli, R. V., Joyner, T.A., Reynolds, S.J., Ballinger, T.J., 2015b. Overlap of global  
753 Köppen–Geiger climates, biomes, and soil orders. *Phys. Geogr.* 36, 158–175.  
754 <https://doi.org/10.1080/02723646.2015.1016384>

755 Rubel, F., Kottek, M., 2010. Observed and projected climate shifts 1901-2100  
756 depicted by world maps of the Köppen-Geiger climate classification. *Meteorol.*  
757 *Zeitschrift* 19, 135–141. <https://doi.org/10.1127/0941-2948/2010/0430>

758 Schaaf, C.B., Gao, F., Strahler, A.H., Lucht, W., Li, X., Tsang, T., Strugnell, N.C.,  
759 Zhang, X., Jin, Y., Muller, J., Lewis, P., Barnsley, M., Hobson, P., Disney, M.,  
760 Roberts, G., Dunderdale, M., Doll, C., Robert, P., Hu, B., Liang, S., Privette,  
761 J.L., Roy, D., 2002. First operational BRDF, albedo nadir reflectance products  
762 from MODIS 83, 135–148.

763 Scheffer, M., Carpenter, S., Foley, J.A., Folke, C., Walker, B., 2001. Catastrophic  
764 shifts in ecosystems. *Nature* 413, 591–596. <https://doi.org/10.1038/35098000>

765 Shen, M., Piao, S., Jeong, S.-J., Zhou, L., Zeng, Z., Ciais, P., Chen, D., Huang, M.,  
766 Jin, C.-S., Li, L.Z.X., Li, Y., Myneni, R.B., Yang, K., Zhang, G., Zhang, Y.,  
767 Yao, T., 2015. Evaporative cooling over the Tibetan Plateau induced by  
768 vegetation growth. *Proc. Natl. Acad. Sci.* 112, 9299–9304.  
769 <https://doi.org/10.1073/pnas.1504418112>

770 Stark, S.C., Breshears, D.D., Garcia, E.S., Law, D.J., Minor, D.M., Saleska, S.R.,  
771 Swann, A.L.S., Villegas, J.C., Aragão, L.E.O.C., Bella, E.M., Borma, L.S.,

772 Cobb, N.S., Litvak, M.E., Magnusson, W.E., Morton, J.M., Redmond, M.D.,  
773 2016. Toward accounting for ecoclimate teleconnections: intra- and inter-  
774 continental consequences of altered energy balance after vegetation change.  
775 *Landscl. Ecol.* 31, 181–194. <https://doi.org/10.1007/s10980-015-0282-5>

776 Sunday, J.M., Bates, A.E., Dulvy, N.K., 2011. Global analysis of thermal tolerance  
777 and latitude in ectotherms. *Proc. R. Soc. B Biol. Sci.* 278, 1823–1830.  
778 <https://doi.org/10.1098/rspb.2010.1295>

779 Tucker, C.J., Pinzon, J.E., Brown, M.E., Slayback, D.A., Pak, E.W., Mahoney, R.,  
780 Vermote, E.F., El Saleous, N., 2005. An extended AVHRR 8-km NDVI dataset  
781 compatible with MODIS and SPOT vegetation NDVI data. *Int. J. Remote Sens.*  
782 26, 4485–4498. <https://doi.org/10.1080/01431160500168686>

783 Turco, M., Von Hardenberg, J., AghaKouchak, A., Llasat, M.C., Provenzale, A.,  
784 Trigo, R.M., 2017. On the key role of droughts in the dynamics of summer fires  
785 in Mediterranean Europe. *Sci. Rep.* 7, 1–10. [https://doi.org/10.1038/s41598-017-](https://doi.org/10.1038/s41598-017-00116-9)  
786 00116-9

787 Wang, M., Overland, J.E., 2004. Detecting arctic climate change using Köppen  
788 climate classification. *Clim. Change* 67, 43–62. [https://doi.org/10.1007/s10584-](https://doi.org/10.1007/s10584-004-4786-2)  
789 004-4786-2

790 Williams, J.W., Jackson, S.T., Kutzbach, J.E., 2007. Projected distributions of novel  
791 and disappearing climates by 2100 AD. *Proc. Natl. Acad. Sci. U. S. A.* 104,  
792 5738–5742. <https://doi.org/10.1073/pnas.0606292104>

793 Wu, D., Zhao, X., Liang, S., Zhou, T., Huang, K., Tang, B., Zhao, W., 2015. Time-lag

794 effects of global vegetation responses to climate change. *Glob. Chang. Biol.* 21,  
795 3520–3531. <https://doi.org/10.1111/gcb.12945>

796 Wu, J., 2004. Effects of changing scale on landscape pattern analysis: Scaling  
797 relations. *Landscape Ecol.* 19, 125–138.  
798 <https://doi.org/10.1023/B:LAND.0000021711.40074.ae>

799 Yang, Y., Roderick, M.L., Zhang, S., McVicar, T.R., Donohue, R.J., 2018.  
800 Hydrologic implications of vegetation response to elevated CO<sub>2</sub> in climate  
801 projections. *Nat. Clim. Chang.* <https://doi.org/10.1038/s41558-018-0361-0>

802 Zhao, Y., 2018. Vegetation and climate reconstructions on different time scales in  
803 China: a review of Chinese palynological research. *Veg. Hist. Archaeobot.* 27,  
804 381–392. <https://doi.org/10.1007/s00334-017-0655-6>

805 Zhao, Y., Herzschuh, U., Li, Q., 2015. Complex vegetation responses to climate  
806 change on the Tibetan Plateau: A paleoecological perspective. *Natl. Sci. Rev.* 2,  
807 400–402. <https://doi.org/10.1093/nsr/nwv057>

808 Zhu, X., Li, Y., Li, M., Pan, Y., Shi, P., 2013. Agricultural irrigation in China. *J. Soil  
809 Water Conserv.* 68, 147–154. <https://doi.org/10.2489/jswc.68.6.147A>

810

811 **Figure 1.** Distribution of (a) annual average temperature (China's ground temperature  
812 0.5° × 0.5° grid dataset) (<http://data.cma.cn/data/index/>), (b) annual average  
813 precipitation (China's ground precipitation 0.5° × 0.5° grid dataset), (c) topography



814 (SRTM DEM) (<http://www.gscloud.cn/>), and (d) vegetation types extracted from year  
815 2000 land cover data (<http://www.resdc.cn/>) in China.

816 **Figure 2.** Trends in (a) annual average temperature and (b) precipitation and  
817 correlations of NDVI to (c) temperature and (d) precipitation during 1982–2012.

818 **Figure 3.** The spatial distribution of the Köppen climate zones in China for (a) 1982,  
819 (b) 1990, (c) 2000, and (d) 2010. Each year represents an average period of five  
820 consecutive years. A–E represents tropical, arid, temperate, continental, and alpine  
821 climates, respectively. During 1990–2000, shifts between continental and arid  
822 climates predominantly occurred in the Northeast Plain.

823 **Figure 4.** Cumulative percentage of area change of all climate zones in China during  
824 1983–2012. The temporal trend was statistically significant at the significance level of  
825 0.05, based on the MK test.

826 **Figure 5.** Temporal variations of percentage area for (a) arid, (b) temperate, (c)  
827 continental, and (d) alpine zones in China during 1982–2012. Changes in climatic  
828 type percentage areas are based on 5-yr running means of ground temperature and  
829 precipitation  $0.5^\circ \times 0.5^\circ$  grid datasets. Note that the y-axis scale differs between  
830 climatic zones.

831 **Figure 6.** Sensitivity analysis of (a) arid, (b) temperate, (c) continental, and (d) alpine  
832 zones.  $S_{\text{precip}}$  and  $S_{\text{temp}}$  represent the sensitivity analysis results with precipitation or  
833 temperature held constant, respectively. The results show that precipitation is the  
834 dominant driver in the arid and continental climate zones, while temperature is the  
835 dominant driver in the temperate and alpine climate zones. All fittings were

836 statistically significant ( $p < 0.01$ , t-test). Note that the axis scale differs between  
837 climatic zones.

838 **Figure 7.** Trends in (a) surface SW content (ERA-interim), (b) NDVI (GIMMS), (c)  
839 albedo (ERA-interim), and (d) the correlation between albedo and NDVI from 1982  
840 to 2012. Statistically significant correlations ( $p < 0.05$ ) are marked with crosses.

841 **Figure 8.** The response of the percentage area (PA) to its dominant climate control  
842 (temperature or precipitation) in (a) arid, (b) temperate, (c) continental, and (d) alpine  
843 climate zones from 1982 to 2012. The percentage area is indicated by the location of  
844 circles, while mean NDVI is indicated by the colour of the circles. Changes in  
845 percentage area are negatively correlated to precipitation in arid climate and to  
846 temperature in alpine climate, while percentage area change is positively correlated to  
847 temperature in temperate climate and to precipitation in continental climate. The  
848 histograms indicate changes in the surface SW anomaly.

849 **Figure 9.** The relationship between annual NDVI (red lines) and albedo (blue line)  
850 from 1982 to 2012.

851 **Figure 10.** Monthly trends in NDVI, albedo, and SW anomaly for (a) arid, (b)  
852 temperate, (c) continental, and (d) alpine climate zone during 1982–2012. The green  
853 shaded areas represent the growing period (Arid: May to October; Temperate: April to  
854 November; Continental: May to mid-October; Alpine: May to mid-September). The  
855 clear monthly trends in NDVI, albedo, and SW content occur during the growing

856 period. The temporal trend was statistically significant at the significance level of  
857 0.05, based on the MK test.

858 **Table 1.** Remote sensing and meteorological reanalysis dataset characteristics

859 **Table 2.** Changes in percentage area of different periods relative to baseline time  
860 (1982).

861 **Table 3.** Qualitative sensitivity parameters of the percentage area in each climate  
862 zone where either temperature or precipitation is held constant.

## Tables

**Table 1.** Remote sensing and meteorological reanalysis dataset characteristics

Data type	Product	Version	Spatial resolution	Temporal resolution	Timestep
NDVI	GIMSS NDVI3g	V0	0.0833° × 0.0833°	Half month	1982–2012
Temperature	China's ground temperature 0.5° × 0.5° Grid data set	V2.0	0.5° × 0.5°	Monthly	1982–2012
Precipitation	China's ground precipitation 0.5° × 0.5° Grid data set	V2.0	0.5° × 0.5°	Monthly	1982–2012
Albedo	ERA-Interim	V2.0	0.125° × 0.125°	Monthly	1982–2012
Volumetric soil water	ERA-Interim	V2.0	0.125° × 0.125°	Monthly	1982–2012
Topography	SRTM DEM	\	1 km	\	2000
Vegetation type	Land use/cover (2000)	\	1 km	\	2000

**Table 2.** Changes in percentage area of different periods relative to baseline time (1982).

Comparison	Arid	Temperate	Continental	Alpine
$\Delta PA_{1990}$	-1.10	1.34	0.20	-0.47
$\Delta PA_{2000}$	3.01	0.95	-3.72	-0.33
$\Delta PA_{2010}$	-1.74	0.24	1.95	-0.50

**Table 3.** Qualitative sensitivity parameters of the percentage area in each climate zone where either temperature or precipitation is held constant.

Zones	Sensitivity parameter	Linear regression equation	Coefficients of determination ( $r^2$ )	Significance ( $p$ )
B	$S_{precip}$	$y = 0.74x + 7.73$	<b>0.856</b>	<b><math>p &lt; 0.01</math></b>
	$S_{temp}$	$y = 0.3x + 19.58$	0.473	$p < 0.01$
C	$S_{precip}$	$y = 0.13x + 20.18$	0.646	$p < 0.01$
	$S_{temp}$	$y = 0.95x + 1.39$	<b>0.980</b>	<b><math>p &lt; 0.01</math></b>
D	$S_{precip}$	$y = 0.59x + 11.12$	<b>0.815</b>	<b><math>p &lt; 0.01</math></b>
	$S_{temp}$	$y = 0.49x + 17.21$	0.753	$p < 0.01$
E	$S_{precip}$	$y = -1.31x + 40.57$	0.514	$p < 0.01$
	$S_{temp}$	$y = 1.28x - 5.47$	<b>0.968</b>	<b><math>p &lt; 0.01</math></b>

B–E represent arid, temperate, continental, and alpine climates, respectively.

**Figure 1.** Distribution of (a) annual average temperature (China's ground temperature  $0.5^\circ \times 0.5^\circ$  grid dataset) (<http://data.cma.cn/data/index/>), (b) annual average precipitation (China's ground precipitation  $0.5^\circ \times 0.5^\circ$  grid dataset), (c) topography (SRTM DEM) (<http://www.gscloud.cn/>), and (d) vegetation types extracted from year 2000 land cover data (<http://www.resdc.cn/>) in China.

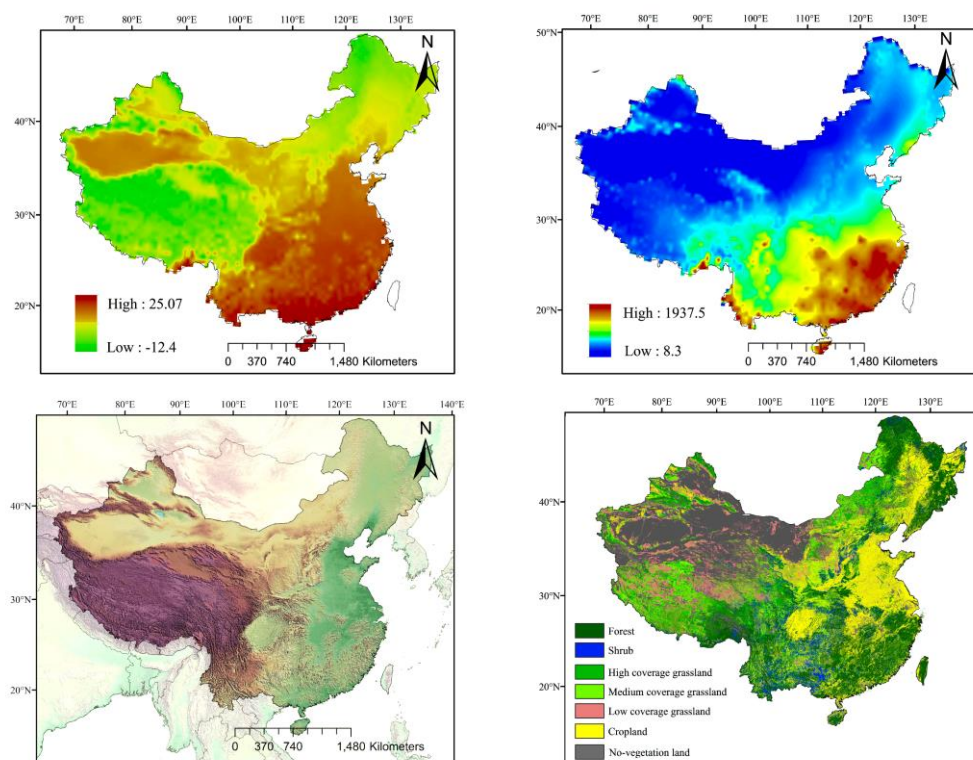


**Figure 2.** Trends in (a) annual average temperature and (b) precipitation and correlations of NDVI to (c) temperature and (d) precipitation during 1982–2012.

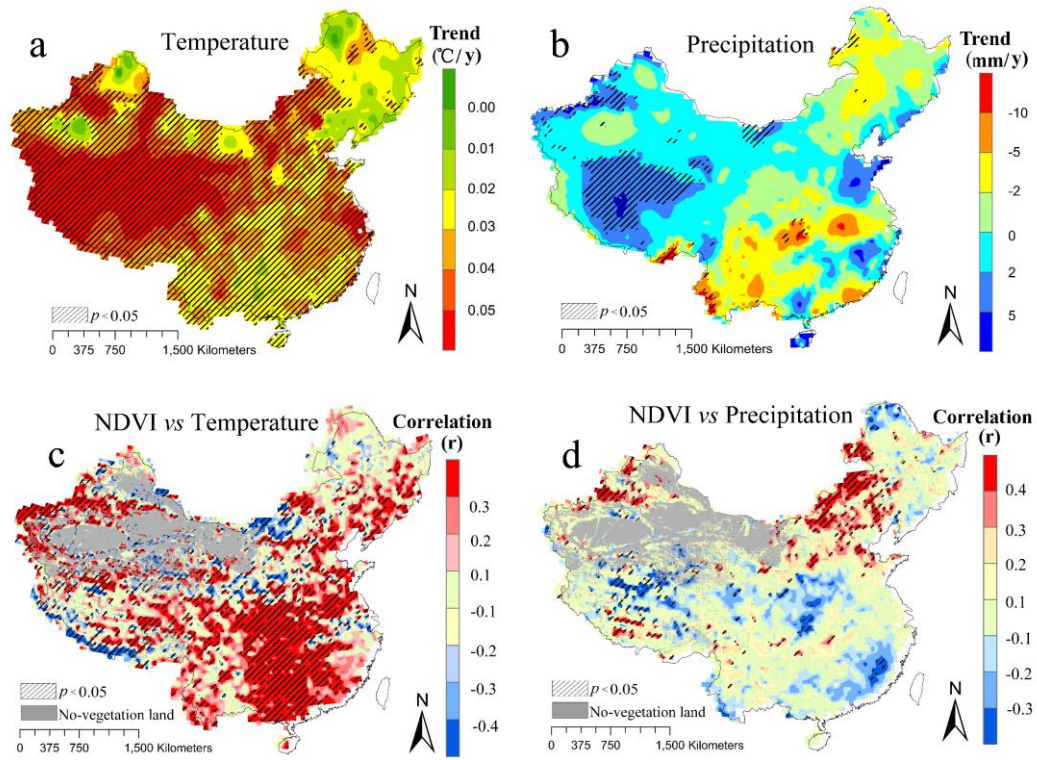


**Figure 3.** The spatial distribution of the Köppen climate zones in China for (a) 1982, (b) 1990, (c) 2000, and (d) 2010. Each year represents an average period of five consecutive years. A–E represents tropical, arid, temperate, continental, and alpine climates, respectively. During 1990–2000, shifts between continental and arid climates predominantly occurred in the Northeast Plain.

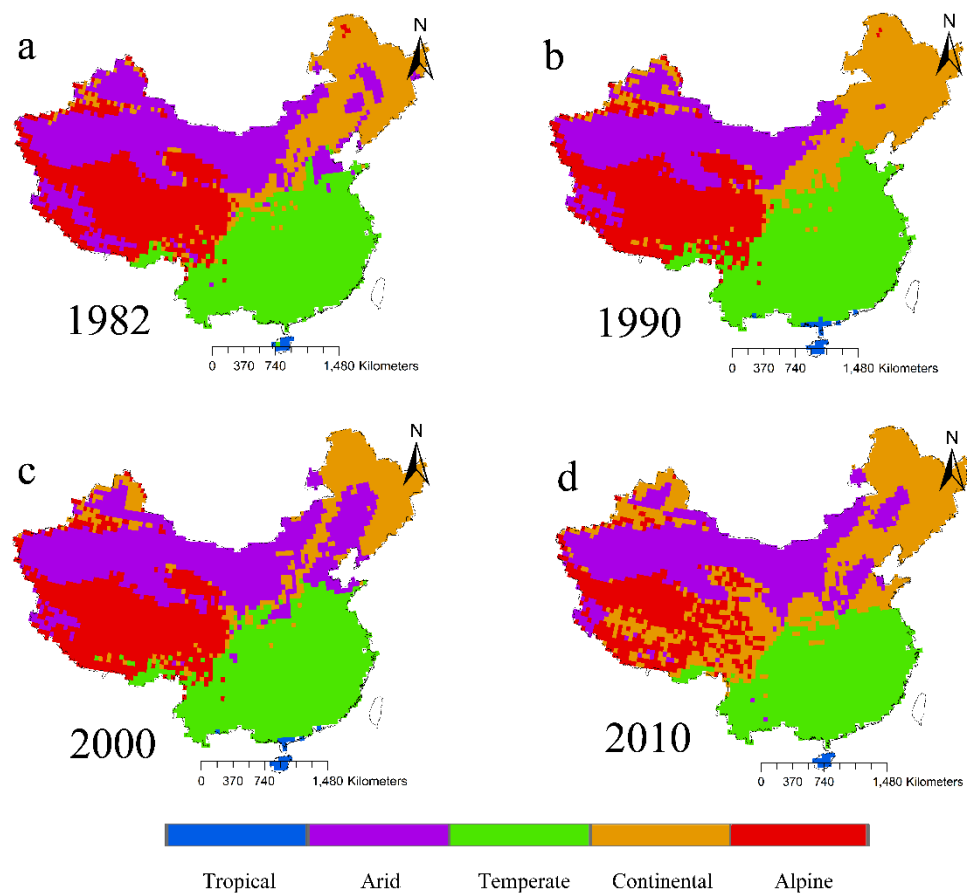




**Figure 4.** Cumulative percentage of area change of all climate zones in China during 1983–2012. The temporal trend was statistically significant at the significance level of 0.05, based on the MK test.

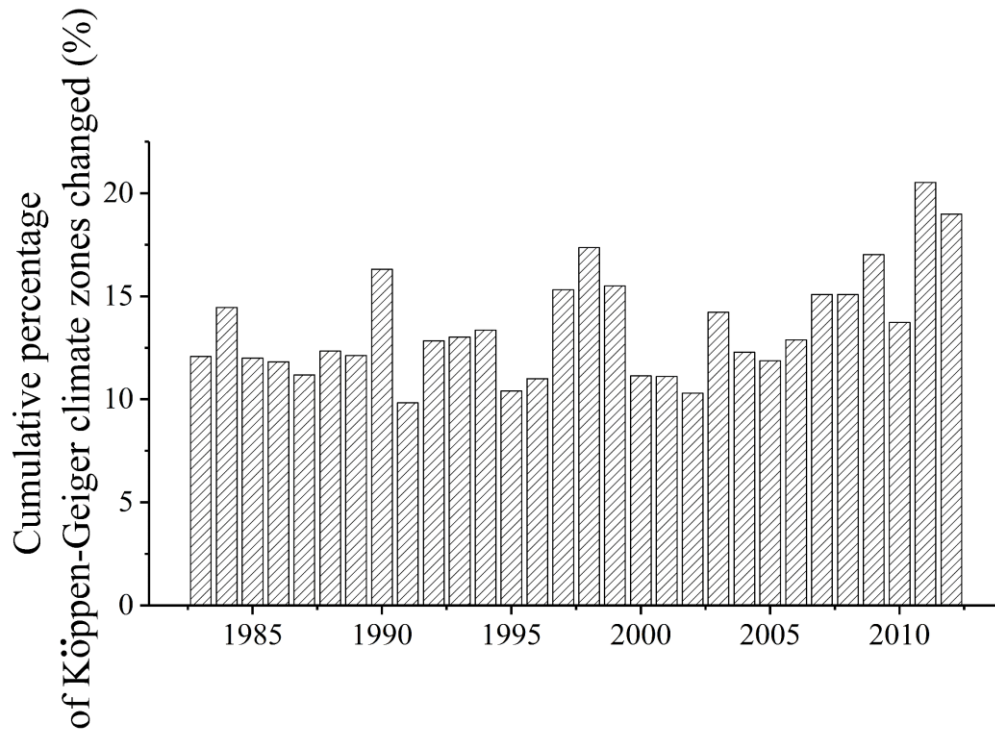


**Figure 5.** Temporal variations of percentage area for (a) arid, (b) temperate, (c) continental, and (d) alpine zones in China during 1982–2012. Changes in climatic type percentage areas are based on 5-yr running means of ground temperature and precipitation  $0.5^\circ \times 0.5^\circ$  grid datasets. Note that the y-axis scale differs between climatic zones.

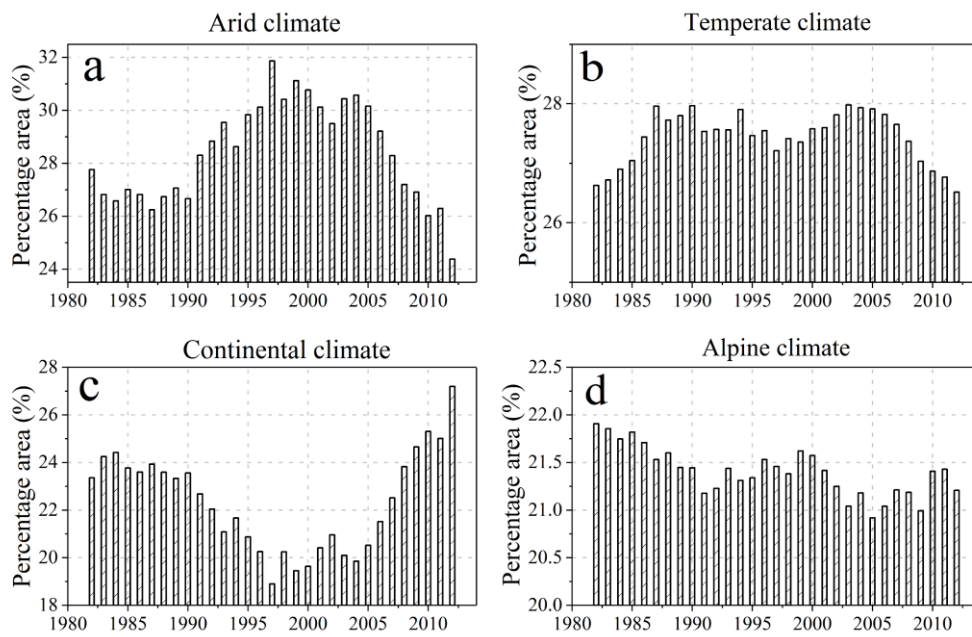


**Figure 6.** Sensitivity analysis of (a) arid, (b) temperate, (c) continental, and (d) alpine zones.  $S_{\text{precip}}$  and  $S_{\text{temp}}$  represent the sensitivity analysis results with precipitation or temperature held constant, respectively. The results show that precipitation is the dominant driver in the arid and continental climate zones, while temperature is the dominant driver in the temperate and alpine climate zones. All fittings were statistically significant ( $p < 0.01$ , t-test). Note that the axis scale differs between climatic zones.

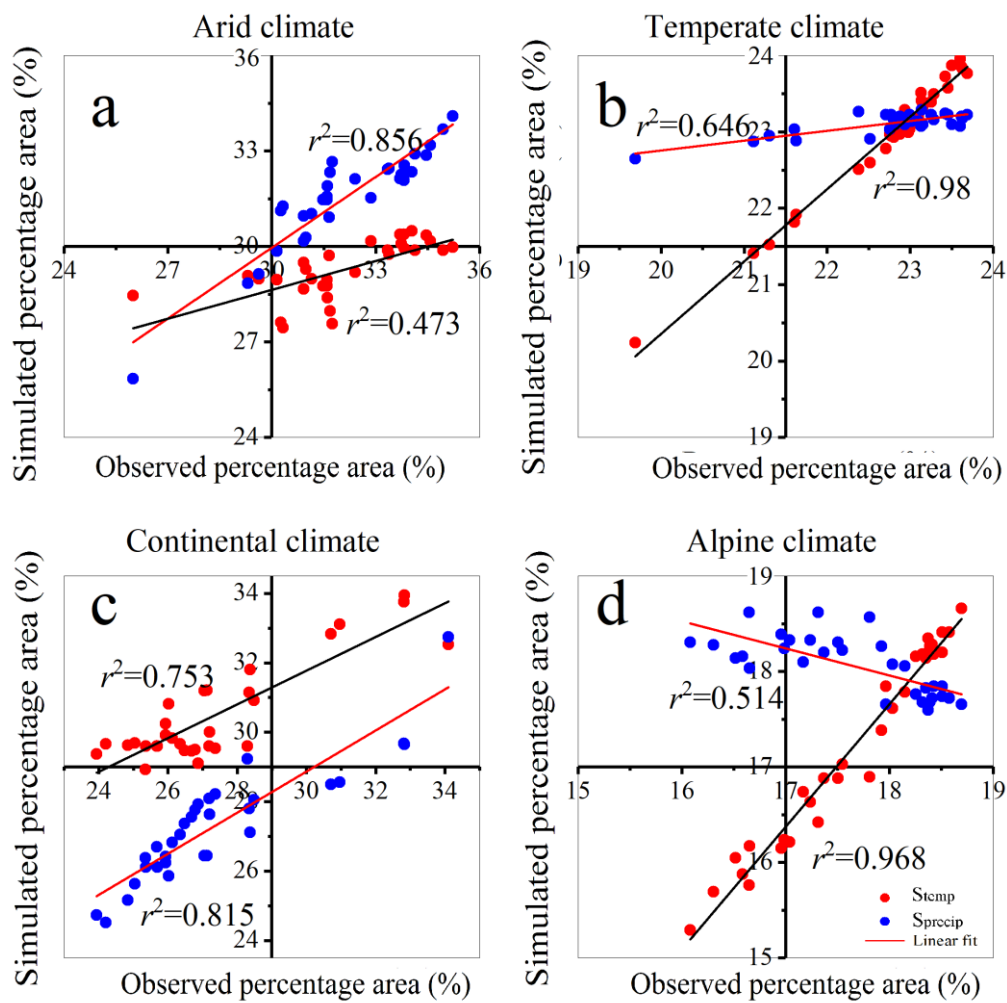


**Figure 7.** Trends in (a) surface SW content (ERA-interim), (b) NDVI (GIMMS), (c) albedo (ERA-interim), and (d) the correlation between albedo and NDVI from 1982 to 2012. Statistically significant correlations ( $p < 0.05$ ) are marked with crosses.

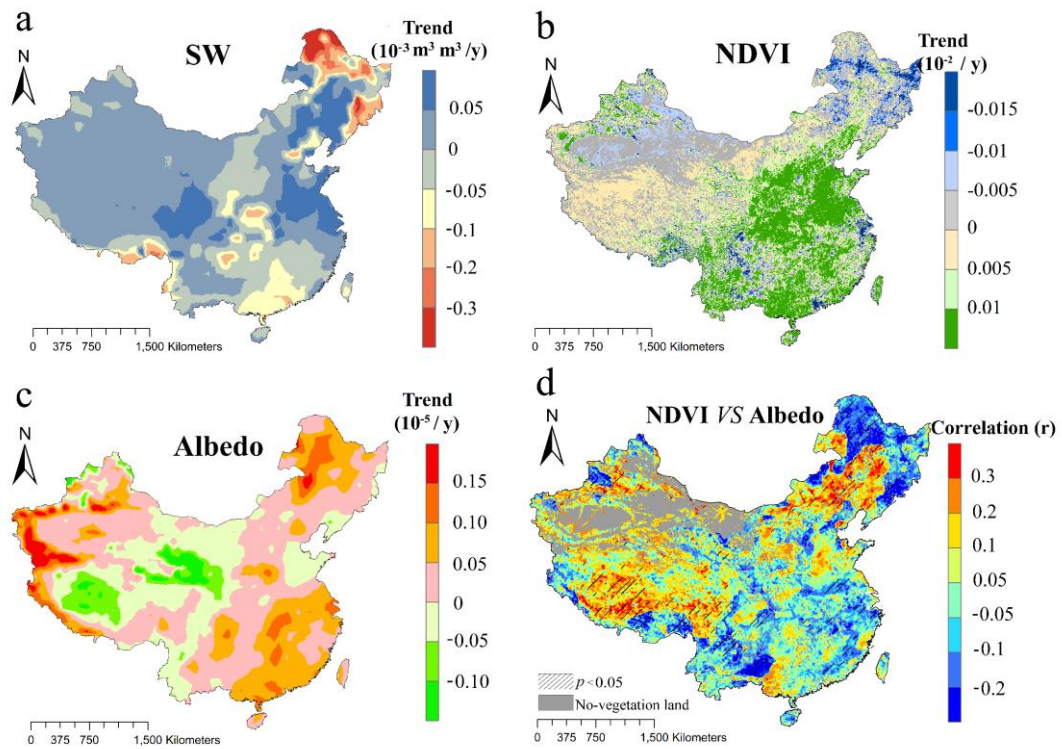


**Figure 8.** The response of the percentage area (PA) to its dominant climate control (temperature or precipitation) in (a) arid, (b) temperate, (c) continental, and (d) alpine climate zones from 1982 to 2012. The percentage area is indicated by the location of circles, while mean NDVI is indicated by the colour of the circles. Changes in percentage area are negatively correlated to precipitation in arid climate and to temperature in alpine climate, while percentage area change is positively correlated to temperature in temperate climate and to precipitation in continental climate. The histograms indicate changes in the surface SW anomaly.

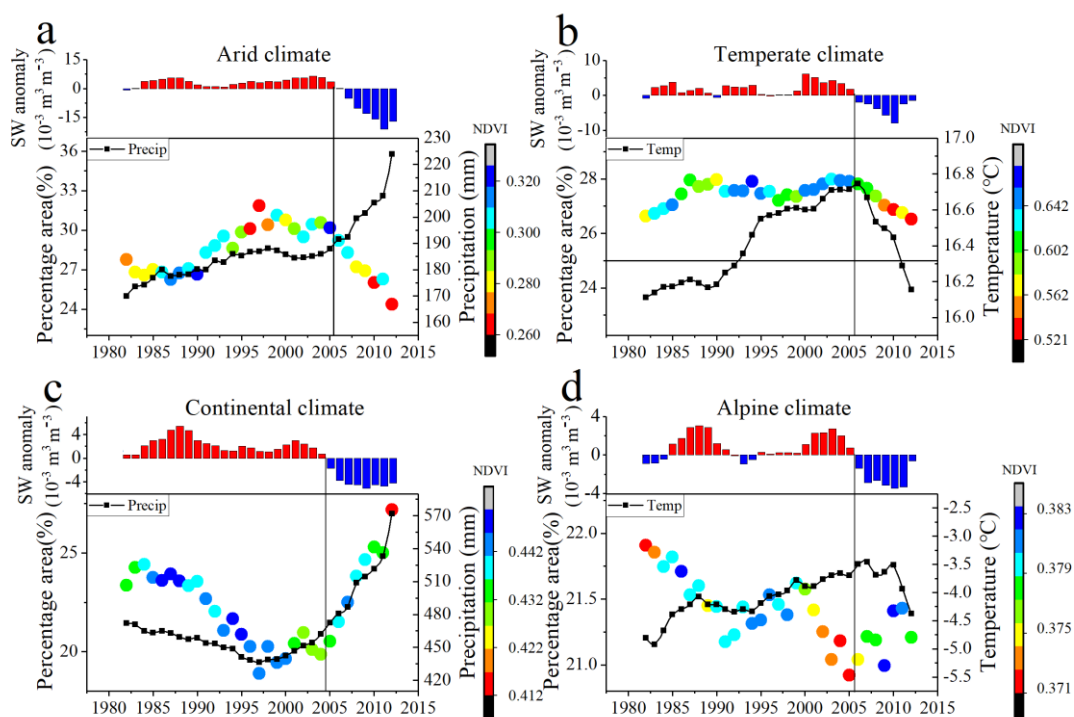


**Figure 9.** The relationship between annual NDVI (red lines) and albedo (blue line) from 1982 to 2012.

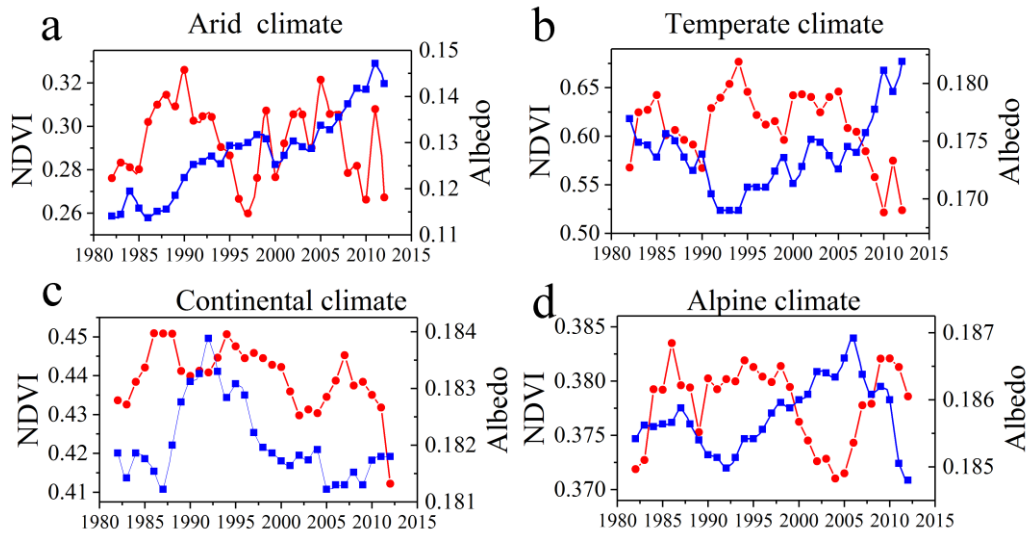


**Figure 10.** Monthly trends in NDVI, albedo, and SW anomaly for (a) arid, (b) temperate, (c) continental, and (d) alpine climate zone during 1982–2012. The green shaded areas represent the growing period (Arid: May to October; Temperate: April to November; Continental: May to mid-October; Alpine: May to mid-September). The clear monthly trends in NDVI, albedo, and SW content occur during the growing period. The temporal trend was statistically significant at the significance level of 0.05, based on the MK test.

